J Biomol NMR (2011) 51:5–19
DOI 10.1007/s10858-011-9537-x

ARTICLE

Dissecting electrostatic interactions in *Bacillus circulans* xylanase through NMR-monitored pH titrations

Lawrence P. McIntosh · Daigo Naito · Simon J. Baturin · Mark Okon · Manish D. Joshi · Jens E. Nielsen

Received: 27 April 2011 / Accepted: 25 June 2011
© Springer Science+Business Media B.V. 2011

Abstract NMR-monitored pH titration curves of proteins provide a rich source of structural and electrostatic information. Although relatively straightforward to measure, interpreting pH-dependent chemical shift changes to obtain site-specific acid dissociation constants (pK_A values) is challenging. In order to analyze the biphasic titrations exhibited by the side chain $^{13}C^{\gamma}$ nuclei of the nucleophilic Glu78 and general acid/base Glu172 in *Bacillus circulans* xylanase, we have revisited the formalism for the ionization equilibria of two coupled acidic residues. In general, fitting NMR-monitored pH titration curves for such a system will only yield the two macroscopic pK_A values that reflect the combined effects of both deprotonation reactions. However, through the use of mutations complemented with ionic strength-dependent measurements, we are able to extract the four microscopic pK_{Ai} values governing the branched acid/base equilibria of Glu78 and Glu172 in BcX. These data, confirmed through theoretical calculations, help explain the pH-dependent mechanism of this model GH11 xylanase by demonstrating that the kinetically determined pK_A values and hence catalytic roles of these two residues result from their electrostatic coupling.

Keywords Acid–base equilibria · Glycoside hydrolase · pH-dependent chemical shift · pH titration · Protein electrostatics

Introduction

Electrostatic interactions are paramount to protein structure, dynamics, and function. These interactions are determined primarily by the ionizable termini and side chains of their constituent amino acid residues, and thus are pH dependent. Accordingly, measurement of the acid dissociation equilibrium constants (pK_A values) of these moieties provides experimental insights into the electrostatic properties of proteins or protein complexes (Creighton 2010).

NMR spectroscopy is certainly the most powerful technique for dissecting pH-dependent phenomena at a molecular level. Using multidimensional heteronuclear NMR techniques, it is generally straightforward to monitor the chemical shift changes of ^{1}H, ^{13}C, and ^{15}N nuclei within a well-behaved protein of small to moderate size in response to the pH titrations of its ionizable groups (Oda et al. 1994; Andre et al. 2007). Although the resulting titration curves are potentially a rich source of structural and electrostatic information (Nielsen 2009), interpreting these data to obtain residue-specific pK_A values remains a challenge (Szakacs et al. 2004). In particular, titration curves often deviate from a simple monophasic dependence on sample pH as expected for a single deprotonation event describable by the Henderson-Hasselbalch equation.

Electronic supplementary material The online version of this article (doi:10.1007/s10858-011-9537-x) contains supplementary material, which is available to authorized users.

L. P. McIntosh (✉) · D. Naito · S. J. Baturin · M. Okon · M. D. Joshi
Department of Biochemistry and Molecular Biology, Department of Chemistry, and Michael Smith Laboratories, Life Sciences Centre, University of British Columbia, 2350 Health Sciences Mall, Vancouver, BC V6T 1Z3, Canada
e-mail: mcintosh@chem.ubc.ca

J. E. Nielsen
School of Biomolecular and Biomedical Science, Centre for Synthesis and Chemical Biology, UCD Conway Institute, University College Dublin, Belfield, Dublin 4, Ireland

This results from the complex nature of electrostatic interactions within a protein, combined with the exquisite sensitivity of chemical shifts to many pH-dependent factors (Buckingham 1960; Hass et al. 2008; Tomlinson et al. 2010; Webb et al. 2011). Accordingly, a wide variety of methods, ranging from residue-specific use of the Henderson-Hasselbalch equation to global spectral fitting in terms of decoupled quasi-site representations (Onufriev et al. 2001) and statistical mechanical models (Sondergaard et al. 2008), have been applied to analyze NMR-detected pH titration curves.

In this paper, we revisit the formalism for analyzing the acid/base equilibria of two interacting ionizable groups with pH-dependent chemical shifts deviating from a single Henderson-Hasselbalch relationship (Shrager et al. 1972). Despite the apparent simplicity of such a system, their NMR-monitored titration curves will generally yield only *macroscopic* acid dissociation constants (pK_{AI} and pK_{AII} values) that represent the collective behavior of both groups. However, under favorable circumstances, *microscopic* pK_{Ai} values ($i = 1$–4) can be extracted from biphasic titration curves, thereby providing a direct measure of the branched deprotonation equilibria of the two moieties and hence their associated electrostatic interaction energy. This is demonstrated through an analysis of *Bacillus circulans* xylanase (BcX), a GH11 family retaining glycoside hydrolase that exploits a nucleophile (Glu78) and a general acid/base (Glu172) to carry out a double displacement hydrolytic mechanism (McIntosh et al. 1996; Joshi et al. 2001). Using mutational analyses to provide limiting chemical shift restraints, pH titrations carried out as a function of ionic strength, and theoretical pK_A calculations, we confirm that the biphasic titration curves of Glu78 and Glu172 result from their electrostatic coupling. This coupling is key to the different charges, and hence enzymatic roles, of the two residues in the catalytically competent protonation state of BcX.

Materials and methods

Protein expression

BcX samples, selectively labeled with $^{13}C^{\delta}$-Glu or uniformly labeled with ^{15}N and ^{13}C, were expressed and purified as described previously (McIntosh et al. 1996; Joshi et al. 2001).

NMR-monitored pH titrations

The pH-dependent chemical shifts of the sidechain carboxyl groups of uniformly $^{13}C/^{15}N$-labeled BcX ($\sim$0.7 mM) were measured using a $H_2(C)CO$ experiment recorded at 25°C with a Varian Inova 600 MHz NMR spectrometer (Kay 1993; Oda et al. 1994). The protein samples were exchanged via a 3000 MWCO Millipore centrifugal filter into a 5% D_2O buffer of 10 mM Na_2HPO_4 and 10 mM sodium d_3-acetate, without (initial ionic strength $\sim$ 40 mM) or with 500 mM NaCl (ionic strength $\sim$ 540 mM). DSS (4,4-dimethyl-4-silapentane-1-sulfonic acid; 1 mM) was included as an internal ^1H and ^{13}C reference. The samples, initially at pH $\sim$ 8.5, were titrated by addition of 0.1 M HCl in microlitre aliquots. This resulted in a total increase of $\sim$40 mM in ionic strength over the course of the titration. Sample pH values were measured at room temperature ($\sim$21°C), and not corrected for temperature or isotope effects. Some precipitated protein formed at lower pH values and was removed by centrifugation. Each spectrum was acquired in $\sim$1 to 2 h and processed using NMRPipe (Delaglio et al. 1995) and Sparky (Goddard and Kneller 2004).

Data analysis

Experimental and theoretical titration curves were simulated or fit to the equations outlined herein using MathWorks Matlab, KaleidaGraph, or GraphPad Prism. The precision of each fit was estimated via a 200–500 step Monte Carlo approach involving random variation of both the pH values ($\pm$0.05 units) and back-calculated ^{13}C chemical shifts ($\pm$0.05 ppm) or charges ($\pm$0.05 units). Model selection was based on an f-test analysis and visual inspection of the data.

Theoretical electrostatic calculations

pK_A calculations were carried out using (1) a combination of automated and manual scripts implemented in WHAT IF to construct optimized hydrogen bonding networks for each ionization state of a given residue, as well as to allow flipping of asparagine, glutamine, and histidine sidechains by 180° about their $\chi 2$, $\chi 3$, or $\chi 2$ dihedral angles, respectively (Hooft et al. 1996); (2) DELPHI to solve the finite-difference Poisson-Boltzmann equation, with uniform dielectric constants of 8 and 80 for the protein and bulk solvent, respectively, an ionic strength of 50 mM, and a temperature of 25°C (Yang et al. 1993); and (3) a Monte-Carlo sampling of the Boltzmann distribution describing the interactions of all ionizable groups in order to calculate the fractional protonation of each as a function of pH (Nielsen et al. 1999; Nielsen 2009). Pertinent model pK_A values were Asp (4.0), Glu (4.4), C-terminus (3.8), and His (6.3).

Results

Theory

The analysis of the NMR titration curves for a system of two ionizable groups follows the formalism of (Edsall and Wyman 1958) and (Shrager et al. 1972). (See also (Rabenstein and Sayer 1976b) and (Szakacs et al. 2004).) One rarely detects the ionizable proton directly, but rather observes the signal from a non-exchangeable nucleus, usually within or adjacent to given residue, whose shift is dependent upon the protonation state of that residue. Thus, in specific reference to this study of BcX, we discuss the case of two glutamic (or aspartic) acids whose titrations are monitored via their side chain carboxyl δ-(or γ-) ^{13}C nuclei. The ionization of these acidic residues acid typically dominates the pH-dependent chemical shift changes of their carboxyl $^{13}C^{\gamma/\delta}$ (Quirt et al. 1974; Batchelor et al. 1975; Rabenstein and Sayer 1976a; Surprenant et al. 1980). However, this is general for any observable nuclei in a pair of ionizable groups, as well as for nuclei in non-ionizable side chains whose chemical shifts are dependent upon the protonation states of two ionizable groups. The carboxylic acid groups may interact either "thermodynamically," whereby the dissociation constant of one depends on the ionization state of the other, and/or "spectroscopically" in that the chemical shift of one is perturbed by the ionization of the other. The analysis can be extended to binding phenomenon in general, although the requirement of knowing the free rather than total ligand concentration (which is readily provided by a pH-sensitive glass electrode) introduces additional complications into the data fitting procedures (Wang 1995).

A general scheme for two carboxyl groups at sites 1 and 2 in a protein P is shown in Fig. 1. Protonation at site 1 is denoted as H^1 and site 2 as H^2. The site-specific *microscopic* acid dissociation constants K_{Ai} are defined by relationships of the form:

$$K_{A1} = \left[PH^2\right]\left[H^+\right]/\left[PH^1H^2\right] \tag{1}$$

with K_{A1} and K_{A4} corresponding to the loss of a proton from site 1 when site 2 is protonated or deprotonated, respectively. Similarly, K_{A2} and K_{A3} correspond to site 2. Molar concentrations are assumed to accurately reflect thermodynamic activities and charges are not shown except for the hydronium ion, denoted as H^+ for simplicity. Overall $K_{A1}\,K_{A3} = K_{A2}\,K_{A4}$. In the absence of any interaction between the two sites, $K_{A1} = K_{A4}$ and $K_{A2} = K_{A3}$. Otherwise, if the acid dissociation constant for one carboxyl group is influenced by the ionization state of the other, then $K_{A4} = \alpha\,K_{A1}$ and $K_{A3} = \alpha\,K_{A2}$, where α is an interaction or cooperativity factor ($\alpha < 1$ for increased electrostatic repulsion or loss of attraction due to progressive deprotonation; positive cooperativity with $\alpha > 1$ is rarely seen with proteins (Alberty 2000)). This may arise from direct electrostatic interactions or indirectly via conformational changes.

The fraction of the protein in the explicit protonation states a, b, c, and d is given by:

$$\begin{aligned} f_a &= [H^+]^2/\Sigma \\ f_b &= K_{A1}[H^+]/\Sigma \\ f_c &= K_{A2}[H^+]/\Sigma \\ f_d &= K_{A1}K_{A3}/\Sigma \end{aligned} \tag{2}$$

$$\Sigma = [H^+]^2 + K_{A1}[H^+] + K_{A2}[H^+] + K_{A1}K_{A3}$$

The denominator Σ is the binding polynomial (Alberty 2000). Under the commonly observed conditions of fast exchange, the measured $^{13}C^{\delta/\gamma}$ chemical shift of the carboxyl group at site 1, δ_1, is the population-weighted average of the chemical shifts of this group (δ_{a1}, δ_{b1}, δ_{c1}, δ_{d1}) in the four possible protonation states of the protein, as shown in Fig. 1 and expressed in equations (3a, b):

$$\delta_1 = f_a\delta_{a1} + f_b\delta_{b1} + f_c\delta_{c1} + f_d\delta_{d1} \tag{3a}$$

$$\delta_1 = \frac{\left(\delta_{a1}10^{-2(pH)} + \delta_{b1}10^{-(pH+pK_{A1})} + \delta_{c1}10^{-(pH+pK_{A2})} + \delta_{d1}10^{-(pK_{A1}+pK_{A3})}\right)}{\left(10^{-2(pH)} + 10^{-(pH+pK_{A1})} + 10^{-(pH+pK_{A2})} + 10^{-(pK_{A1}+pK_{A3})}\right)} \tag{3b}$$

The changes in the chemical shifts ($\delta_{b1} - \delta_{a1}$) and ($\delta_{d1} - \delta_{c1}$), of the site 1 carboxyl are attributed to its own ionization, whereas deprotonation of the carboxyl at site 2 results in the changes ($\delta_{c1} - \delta_{a1}$) and ($\delta_{d1} - \delta_{b1}$). These spectroscopic changes could arise from factors such as through-bond inductive effects, through-space electric field-induced shielding effects, or conformational perturbations. Similarly, for the carboxyl at site 2:

$$\delta_2 = f_a\delta_{a2} + f_b\delta_{b2} + f_c\delta_{c2} + f_d\delta_{d2} \tag{3c}$$

In this simple system of two ionizable groups, the observed pH-dependent chemical shifts of each carboxyl are potentially a function of four limiting chemical shifts and three independent microscopic acid dissociation

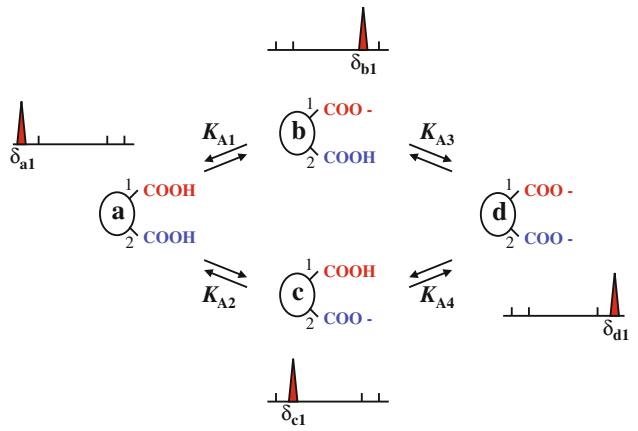

Fig. 1 General scheme for the ionization equilibria of two carboxylic acids in a protein. The four protonation states of these two moieties (*a*, *b*, *c*, *d*) and the associated microscopic acid dissociation equilibrium constants (K_{A1} and K_{A4} for carboxyl 1; K_{A2} and K_{A3} for carboxyl 2) are indicated. By thermodynamic linkage, K_{A1} $K_{A3} = K_{A2}$ K_{A4}, and $K_{A3} = \alpha$ K_{A2} and $K_{A4} = \alpha$ K_{A1}, where α is the interaction factor for coupled ionizations. Also represented arbitrarily are the ^{13}C chemical shifts of carboxyl 1 in these four states (δ_{a1}, δ_{b1}, δ_{c1}, and δ_{d1}). A similar figure can be drawn for carboxyl 2 with shifts δ_{a2}, δ_{b2}, δ_{c2}, and δ_{d2}

constants. However, biphasic titration curves of chemical shift versus pH for each carboxyl can be defined by five variables (e.g. two endpoint and one intermediate chemical shifts, and two apparent pK_A values corresponding to inflection points), and thus (3) is experimentally underdetermined. Since sites 1 and 2 share common pK_{Ai} values, simultaneous analysis of their titration curves can improve the accuracy of the fit parameters, but does not fully resolve this problem (Shrager et al. 1972; Ullmann 2003). Accordingly, in the absence of chemical shift or pK_A restraints from independent measurements, several limiting cases must be considered in order to extract the desired ionization constants from pH-dependent NMR spectra by non-linear least squares analysis.

Case 1: Independent, non-interacting sites.

In the simplest case where the two carboxyl groups titrate independently ($\alpha = 1$) and the chemical shift of each is not influenced by the other, then for site 1, $pK_{A1} = pK_{A4}$, $\delta_{a1} = \delta_{c1}$, and $\delta_{b1} = \delta_{d1}$. In terms of the measured sample pH, (3b) becomes the familiar equation for the monophasic NMR-monitored titration curve of a single ionizable group:

$$\delta_1 = \frac{\delta_{a1}10^{-pH} + \delta_{b1}10^{-pK_{A1}}}{10^{-pH} + 10^{-pK_{A1}}} \tag{4}$$

A similar modified Henderson–Hasselbalch expression can be written for site 2, with $pK_{A2} = pK_{A3}$, $\delta_{a2} = \delta_{b2}$, and $\delta_{c2} = \delta_{d2}$.

Case 2: "Thermodynamically coupled" titrations—Interdependent microscopic pK_{Ai} values with chemical shifts depending only on the individual ionization state of a carboxyl group.

In the case where the two carboxyl groups interact such that the microscopic acid dissociation constant of each residue depends on the ionization state of the other, then $\alpha \neq 1$, and $pK_{A1} \neq pK_{A4}$ and $pK_{A2} \neq pK_{A3}$. However, if the chemical shift changes exhibited by each carboxyl result exclusively from its own ionization, then for site 1, $\delta_{a1} = \delta_{c1}$ and $\delta_{b1} = \delta_{d1}$, and for site 2, $\delta_{a2} = \delta_{b2}$ and $\delta_{c2} = \delta_{d2}$. The pH dependence of the chemical shift of the carboxyl at site 1 is given by equation (5a):

$$\delta_1 = \frac{\delta_{a1}\left(10^{-2(pH)} + 10^{-(pH+pK_{A2})}\right) + \delta_{b1}\left(10^{-(pH+pK_{A1})} + 10^{-(pK_{A1}+pK_{A3})}\right)}{10^{-2(pH)} + 10^{-(pH+pK_{A2})} + 10^{-(pH+pK_{A1})} + 10^{-(pK_{A1}+pK_{A3})}} \tag{5a}$$

From a non-linear least squares fit of the observed chemical shift δ_1 versus pH to this equation, two end-point chemical shifts and three microscopic pK_{Ai} values can be extracted. The fourth is obtained from the relationship $pK_{A1} + pK_{A3} = pK_{A2} + pK_{A4}$. Similarly for site 2, equation (5b) is applicable:

$$\delta_2 = \frac{\delta_{a2}\left(10^{-2(pH)} + 10^{-(pH+pK_{A1})}\right) + \delta_{c2}\left(10^{-(pH+pK_{A2})} + 10^{-(pK_{A2}+pK_{A4})}\right)}{10^{-2(pH)} + 10^{-(pH+pK_{A1})} + 10^{-(pH+pK_{A2})} + 10^{-(pK_{A2}+pK_{A4})}} \tag{5b}$$

Although obtaining three pK_{Ai} values from a biphasic or apparent two-step titration curve may seem non-intuitive,

note that the mid-way "plateaus" correspond to fractional chemical shift changes of:

site 1

$$(\delta_1 - \delta_{a1}) = (\delta_{b1} - \delta_{a1})\left(\frac{K_{A1}}{K_{A1} + K_{A2}}\right) \quad (6a)$$

site 2

$$(\delta_2 - \delta_{a2}) = (\delta_{c2} - \delta_{a2})\left(\frac{K_{A2}}{K_{A1} + K_{A2}}\right) \quad (6b)$$

Thus the fit results are mathematically equivalent to the three chemical shifts and two pK_A values obtained for cases 3 and 4, as discussed below.

Case 3: "Spectroscopically coupled" titrations: Independent microscopic pK_{Ai} values with chemical shifts depending on the ionization states of both carboxyl groups.

In the case where the two carboxyl groups titrate independently ($\alpha = 1$), $K_{A1} = K_{A4}$ and $K_{A2} = K_{A3}$. However, if the chemical shift of each carboxyl depends upon its own ionization state, as well as that of the second carboxyl, then for site 1, $\delta_{a1} \neq \delta_{c1}$ and $\delta_{b1} \neq \delta_{d1}$, and for site 2, $\delta_{a2} \neq \delta_{b2}$ and $\delta_{c2} \neq \delta_{d2}$. The pH-dependent chemical shift of site 1 is given by equation (7):

$$\delta_1 = \frac{\left(\delta_{a1}10^{-2(pH)} + \delta_{b1}10^{-(pH+pK_{A1})} + \delta_{c1}10^{-(pH+pK_{A2})} + \delta_{d1}10^{-(pK_{A1}+pK_{A2})}\right)}{\left(10^{-2(pH)} + 10^{-(pH+pK_{A1})} + 10^{-(pH+pK_{A2})} + 10^{-(pK_{A1}+pK_{A2})}\right)} \quad (7)$$

This equation is underdetermined with six variables and generally cannot be fit robustly, unless additional restraints are included. These include independent knowledge of the chemical shifts of the carboxyl in the various ionization states of the protein, or by assuming additive chemical shift effects, i.e. $\delta_{c1} = \delta_{a1} + (\delta_{d1} - \delta_{b1})$ (Sudmeier and Reilley 1964). However, if one titration pathway in above scheme is preferred significantly, for example with $pK_{A2} > pK_{A1}$, then the equations for sites 1 and 2 reduce to the commonly used expressions for the analysis of sequential titration curves:

$$\delta_1 = \frac{\delta_{a1}10^{-2(pH)} + \delta_{b1}10^{-(pH+pK_{A1})} + \delta_{d1}10^{-(pK_{A1}+pK_{A2})}}{10^{-2(pH)} + 10^{-(pH+pK_{A1})} + 10^{-(pK_{A1}+pK_{A2})}} \quad (8a)$$

$$\delta_2 = \frac{\delta_{a2}10^{-2(pH)} + \delta_{b2}10^{-(pH+pK_{A1})} + \delta_{d2}10^{-(pK_{A1}+pK_{A2})}}{10^{-2(pH)} + 10^{-(pH+pK_{A1})} + 10^{-(pK_{A1}+pK_{A2})}} \quad (8b)$$

Non-linear least squares fitting of the observed titrations to these equations yield three limiting chemical shifts for each carboxyl groups and two acid dissociation constants. Midway "plateaus" in these titration curves occur at δ_{b1} and δ_{b2} for this particular pathway. However, as shown below, the acid dissociation constants derived from fitting to (8) are in effect macroscopic pK values and the midway chemical shifts weighted averages over both singly protonated states.

Case 4: Macroscopic model.

The most general approach to fitting multiphasic titration curves is to consider macroscopic or net acid dissociation constants, which describe the overall behavior of a system (Edsall and Wyman 1958). For the titration of the two carboxyl groups, K_{AI} corresponds to the net dissociation of the first proton and K_{AII} to the second. In terms of the previously defined microscopic ionization constants,

$$K_{AI} = (K_{A1} + K_{A2}) \quad (9a)$$

and

$$(K_{AII})^{-1} = \left[(K_{A3})^{-1} + (K_{A4})^{-1}\right] \quad (9b)$$

$K_{AI}\,K_{AII} = K_{A1}\,K_{A3} = K_{A2}\,K_{A4}$, regardless of whether the groups interact ($\alpha \neq 1$) or not ($\alpha = 1$). If we define state i as that corresponding to a net single deprotonation of the system, then:

$$f_i = (K_{A1} + K_{A2})[H^+]/\Sigma = K_{AI}[H^+]/\Sigma' \quad (10a)$$

where

$$\Sigma' = [H^+]^2 + K_{AI}[H^+] + K_{AI}K_{AII} \quad (10b)$$

The pH-dependence of the chemical shifts of sites 1 and 2 are given by the expressions:

$$\delta_1 = \frac{\delta_{a1}10^{-2(pH)} + \delta_{i1}10^{-(pH+pK_{AI})} + \delta_{d1}10^{-(pK_{AI}+pK_{AII})}}{10^{-2(pH)} + 10^{-(pH+pK_{AI})} + 10^{-(pK_{AI}+pK_{AII})}} \quad (11a)$$

$$\delta_2 = \frac{\delta_{a2}10^{-2(pH)} + \delta_{i2}10^{-(pH+pK_{AI})} + \delta_{d2}10^{-(pK_{AI}+pK_{AII})}}{10^{-2(pH)} + 10^{-(pH+pK_{AI})} + 10^{-(pK_{AI}+pK_{AII})}} \quad (11b)$$

Here, δ_{i1} and δ_{i2} correspond to the chemical shifts of the two residues after the first net titration step. With five variables, these equations will precisely describe the biphasic titration curve of one ionizable group in the

presence of another. In addition to K_{AI} and K_{AII} each being composites of two microscopic dissociation constants, from a comparison to the expanded form of (3), we see that δ_{i1} and δ_{i2} are weighted chemical shifts of the two possible singly protonated species, i.e. for site 1:

$$\delta_{i1}K_{AI} = \delta_{b1}K_{A1} + \delta_{c1}K_{A2} \quad (12)$$

This is because the interconversion between these species (b and c in Fig. 1) is a pH-independent isomerization. Therefore changes in the site-specific chemical shift of either carboxyl can depend upon both ionization events, and thus in the most general case, we measure the macroscopic or averaged properties of the system by NMR spectroscopy. As noted above, expressions (11) have the identical form as for the simplified versions of Case 3 (8), which were derived assuming a significant difference in microscopic pK_{Ai} values and hence sequential ionization of one carboxyl before the second (e.g. $pK_{A1} \sim pK_{AI}$ and $pK_{A2} \sim pK_{AII}$). The difference between the 2 equations is one of physical interpretation, with (11) applying macroscopically to all cases of Scheme 1 and (8) to a specific microscopic example.

The utility of fitting titration curves to macroscopic equilibria can be seen in the easy extension of (11) to systems involving more than two ionizable groups. For example, with three carboxyls, one can describe the pH-dependence of the chemical shift of site 1 as:

$$\delta_1 = \frac{\delta_{3,1}\,10^{-3(pH)} + \delta_{2,1}10^{-(2pH+pK_{AI})} + \delta_{1,1}10^{-(pH+pK_{AI}+pK_{AII})} + \delta_{0,1}10^{-(pK_{AI}+pK_{AII}+pK_{AIII})}}{10^{-3(pH)} + 10^{-(2pH+pK_{AI})} + 10^{-(pH+pK_{AI}+pK_{AII})} + 10^{-(pK_{AI}+pK_{AII}+pK_{AIII})}} \quad (13)$$

where K_{AI} is the net sum of the three microscopic K_{Ai} values governing the dissociation of the first proton, K_{AIII} is the inverse of the sum of the inverses of the three K_{Ai} values for dissociation of the third proton, and $K_{AI}K_{AII}$ is the sum of the products of the first and second microscopic dissociation constants for the three pathways leading to net loss of two protons. The weighted values of the chemical shifts of site 1 in the triple, double, single and zero protonated states of the protein are $\delta_{3,1}$, $\delta_{2,1}$, $\delta_{1,1}$, and $\delta_{0,1}$, respectively. Although straightforward in form, the physical interpretation of these macroscopic pK_A values and chemical shifts in terms of specific or microscopic events can be difficult, except for simple cases such as a predominant ionization pathway with sequential loss of protons at well separated pH values.

Simulated titration curves

A diagnostic feature of equilibria involving two interacting ionizable residues is a plot of chemical shift versus pH that deviates from a simple monophasic Henderson-Hasselbalch titration curve. This plot may appear broadened or clearly biphasic ($\alpha < 1$) or overly steep ($\alpha > 1$). Figure 2 and Supplemental Figures S1 and S2 illustrate this behaviour, showing that such titration curves can arise from the limiting cases 2 and 3, as well as a completely general example of coupled shifts and dissociation constants. The legends to these figures provide details into the fitting of this simulated data according to the micro- and macroscopic models outlined above. Based on the analysis of these error-free test data, several important conclusions can be drawn.

1. With four chemical shifts and three microscopic pK_{Ai} values, a wide range of titration curves are possible for a set of equilibria as simple as that depicted in Fig. 1. Thus, it is not surprising that the NMR spectra of proteins often show complex pH-dependencies.
2. Fitting titration curves with one predominant transition to the simple model of a single ionization (4) will often yield a reasonable estimate of the "major" pK_A value of a residue (or the pH for ~50% deprotonation), provided that the change in chemical shift reflects primarily the ionization of that residue. This is generally true of the carboxyl ^{13}C signal of an aspartic or glutamic acid or the C-terminus of a protein (Batchelor et al. 1975), the imidazole ^{1}H and ^{13}C signals of a histidine (Markley 1975; Blomberg et al. 1977; Pelton et al. 1993), or the ^{15}N signal of a lysine or the N-terminal amine (Andre et al. 2007), yet may not hold for amides or side chain aliphatic nuclei (Tomlinson et al. 2010; Farrell et al. 2010; Webb et al. 2011). Combined with the inevitability of experimental errors, plus the fact that it may not be possible to measure the NMR spectra of a protein over a pH range sufficient to accurately define baselines or deviations from monophasic behavior, this is encouraging for a "first-order" analysis.
3. Analysis of the simulated titration curves according to (11) will yield accurate macroscopic pK_A and chemical shift values for all variations of the general system outlined in Fig. 1. This equation will robustly fit examples of branch equilibria with positive and negative cooperativity, as well as interdependent chemical shifts, given suitable initial non-linear least squares search conditions. The challenge, of course,

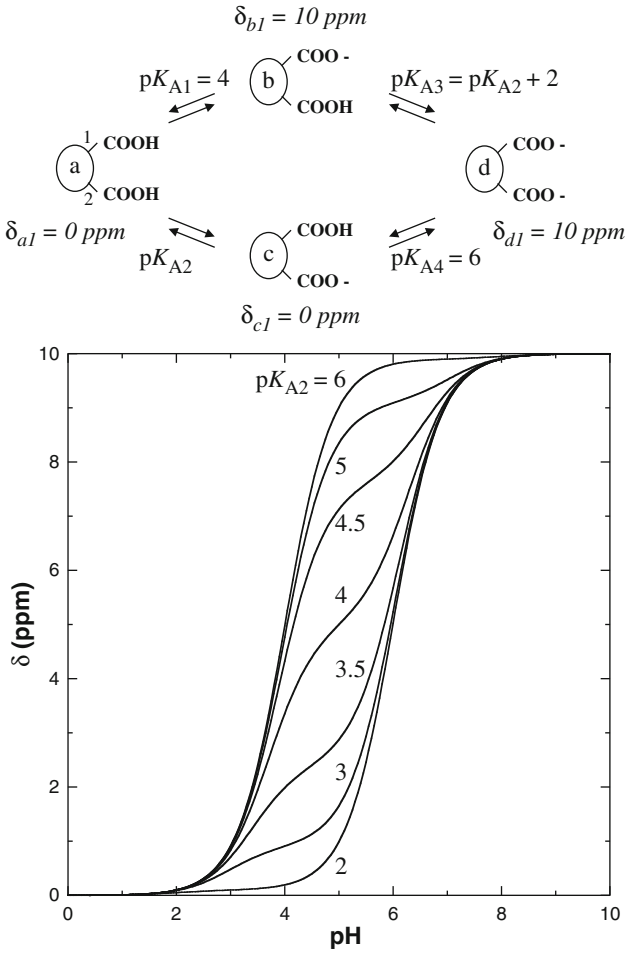

Fig. 2 Simulated chemical shift pH-dependence of a reporter nucleus ▶ in one of two carboxylic acids following case 2 (thermodynamically coupled or branched equilibria with chemical shifts dependent only on the ionization state of the residue itself). Error-free data were generated using (5a) with $(\delta_{d1} - \delta_{a1}) = 10$ ppm and $pK_{A1} = 4$ and $pK_{A4} = 6$ (thus $\alpha = 0.01$) for site 1, along with $pK_{A2} = 2$, 3, 3.5, 4, 4.5, 5, and 6 for site 2. Non-linear least squares fitting to a single Henderson-Hasselbalch titration (4) yields pK_A values of 5.999, 5.958, 5.813, 5.000, 4.188, 4.042, and 4.001, respectively. This reflects the fact that when $pK_{A2} < pK_{A1}$, the system titrates with increasing pH predominantly along the lower branch, as drawn, and thus the "major" pK_A of site 1 is ~6. Conversely, when $pK_{A2} > pK_{A1}$, the upper branch is followed, and the "major" pK_A of site 1 quickly switches to ~4. Although (4) is only fit satisfactorily when $|pK_{A1} - pK_{A2}| \geq 2$ (i.e. the curves are no longer visibly biphasic), even when $|pK_{A1} - pK_{A2}| = 0.5$, the resulting value approximates the "major" pK_A of the residue as well as the pH at which it is ionized in 50% of the molecules present (i.e. "$pK_{A1/2}$"). However, the end point chemical shifts are poorly fit in the latter situation. Fitting to a modified Hill equation (14) yields similar single $pK_{A'}$ values and n values ranging from 0.38 (*middle curve*) to 0.99 (*outer curves*). Despite indicating differing levels of negativity cooperativity, all curves were generated with the same interaction parameter $\alpha = 0.01$. Fitting of the simulated data to (11a) yields macroscopic values of ($\delta_{i1} = 0.099$ ppm, $pK_{AI} = 1.996$, $pK_{AII} = \underline{6.004}$), (0.909 ppm, 2.959, $\underline{6.041}$), (2.403 ppm, 3.381, $\underline{6.119}$), (5.000 ppm, $\underline{3.699}$, $\underline{6.301}$), (7.598 ppm, $\underline{3.881}$, 6.619), (9.090 ppm, $\underline{3.959}$, 7.041), and (9.901 ppm, $\underline{3.996}$, $\underline{8.004}$), respectively. These fit values correspond exactly to the original input data, according to the relationships $\delta_{bi} = (10 \text{ ppm})(K_{A1}/(K_{A1} + K_{A2}))$, $K_{AI} = (K_{A1} + K_{A2})$ and $K_{AII} = ({K_{A3}}^{-1} + {K_{A4}}^{-1})^{-1}$ (6a, 9). The underlined pK_A approximates that of site 1 along its predominant ionization pathway with increasing pH, whereas the other reflects that of site 2. When sites 1 and 2 have the same pK_{Ai} values, the two branches are followed equally and the fit macroscopic values deviate the most (i.e. by $\log(0.5) = -0.301$) from the input microscopic values of $pK_{A1} = pK_{A2} = 4$ and $pK_{A3} = pK_{A4} = 6$

remains to interpret these parameters in terms of microscopic events occurring within a protein (i.e. cases 2 or 3). It is worthy to note that pK_{AI} will always be less that the smaller of the two first microscopic dissociation constants (pK_{A1} or pK_{A2}) while pK_{AII} will always be greater than the larger of the two second microscopic dissociation constants (pK_{A3} or pK_{A4}), yet the deviation will be no more than $\pm\log(2) = \pm 0.3$. This worst case scenario corresponds to the situation where $pK_{A1} = pK_{A2}$ and hence $pK_{A3} = pK_{A4}$, Thus, to a reasonable approximation, macroscopic pK_A values also reflect well the "major" microscopic pK_{Ai} values for the predominant ionization pathway in the coupled system of Fig. 1.

4. Intuitively, biphasic titration curves can be understood in terms of three protonation states of a protein with distinct chemical shifts linked by two ionization events, as discussed for case 3 and exemplified in Supplemental Figure S1. Fitting this simulated data with (7) will yield reliable "major" pK_A values, but often meaningless intermediate chemical shifts (i.e. generally one of the middle terms in this six variable equation will have a negligible contribution to the observed δ). Imposing additional restraints, such as assuming sequential deprotonation events, produces (8), which is identical to (11); thus the extracted parameters are in fact macroscopic pK_A values and weighted chemical shifts. Furthermore, since equations of this form are valid for all permutations of the scheme in Fig. 1, one may miss important aspects of protein electrostatics, such as coupled equilibria, by interpreting NMR-derived titration data in terms of the specific microscopic model of case 3. Distinguishing this model from others requires independent data, such as the knowledge of the chemical shifts of a residue in various protonation states of a protein, for example obtained by characterization of mutant species or through structure-based chemical shift calculations.
5. Although less well appreciated, Fig. 2 illustrates clearly that biphasic NMR titrations can also result from a carboxyl having two microscopic pK_{Ai} values that are dependent upon the protonation state of a second ionizable group. In the limiting situation of case 2,

whereby the chemical shift of a carboxyl is dependent solely upon its own charge, fitting titration data to (5) will yield the four microscopic acid dissociation constants necessary to describe the interactions within this system. However, if its chemical shift is also dependent upon that of the second residue, then we are again restricted to determining macroscopic pK_A values. Evidence for this latter situation is seen most obviously when the chemical shift of a carboxyl both increases and decreases across a titration series (e.g. Supplemental Figure S2). Extracting microscopic constants from these macroscopic parameters will require additional chemical shift or pK_A information, such as that obtained using mutant forms of a protein lacking the coupled ionizable residue. Of course, simultaneous analyses of the titration curves of interacting residues, if both measurable by NMR spectroscopy, can provide important restraints. In particular, coupled sites following case 2 should have "mirror image" titration curves fit with the same microscopic pK_{Ai} values, provided that no significant interactions with other ionizable groups in a protein occur over the pH range considered.

6. As illustrated in Fig. 2, visible deviations from monophasic titrations occur for case 2 only when the two interacting residues have similar pK_{Ai} values in the presence of their protonated partner. Otherwise, their titrations will occur in a predominantly sequential manner with one residue deprotonating before the other regardless of any thermodynamic coupling (Klingen et al. 2006). Based on simulations shown in Supplemental Figure S3, this requires that $|pK_{A1} - pK_{A2}|$ be less than $\sim$1.3 such that the minor branch of Scheme 1 is followed to a measurable extent (i.e. with $K_{A1}/(K_{A1} + K_{A2}) > 0.05$ or < 0.95). If the fit pK_{Al} and pK_{A2} values differ substantially from this limit, then it is physically unreasonable to attribute a biphasic titration curve to coupled ionization equilibria. As a corollary, it is also necessary to measure a titration curve with sufficiently small pH increments and over a wide enough pH range in order to detect deviations from monophasic behaviour and thereby reliably extract information regarding thermodynamic interactions.
7. In situations where NMR-derived titration data deviate from purely monophasic behaviour, yet lack an obvious plateau, fitting is often carried out according to a modified Hill equation (Markley 1975):

$$\delta_1 = \frac{\delta_{1,1}10^{-n(\mathrm{pH})} + \delta_{0,1}10^{-n(\mathrm{p}K_{A'})}}{10^{-n(\mathrm{pH})} + 10^{-n(\mathrm{p}K_{A'})}} \quad (14)$$

Here, $\delta_{1,1}$ and $\delta_{0,1}$ are the chemical shifts of site 1 in its fully protonated and deprotonated states, respectively, $K_{A'}$ is an apparent dissociation constant, and n is the Hill coefficient. When the chemical shift of the site monitored is dependent only upon the ionization state of one moiety (case 2), then fit values of $n < 1$ or >1 reflect negative or positive cooperativity, respectively. Although a physical interpretation of the Hill coefficient has been proposed (Lindman et al. 2006), the quantitative analysis of this parameter is generally difficult. For example, fitting the titration data of Fig. 2 yields values of n ranging from 0.38 for the middle curve to 0.99 for the outer curves, yet all were generated for case 2 using a constant negative interaction term $\alpha = 0.01$. Furthermore, deviations from monophasic titration behaviour can arise without any thermodynamic cooperativity if the chemical shift of one site is simply dependent upon the protonation state of the other. For example, fitting of the data in Supplemental Figure S1 (for case 3 with no interaction term; $\alpha = 1$) to (14) would incorrectly suggest negative cooperativity (n ranging from 0.5 to 1.0). Conversely, fitting of the data in Supplemental Figure S2 would imply positive cooperativity ($n = 1.16$) despite being calculated with a strong negative interaction term of $\alpha = 0.01$. This latter behaviour is due to the chemical shift perturbations from deprotonation at site 2 having the opposite sign as that for site 1, respectively. Thus, the utility of (14) may best lie with simply detecting deviations from ideal monophasic titration behaviour (Rouxfromy 1982).

Coupled titrations of Glu78 and Glu172 in Bcx

BcX provides an excellent example of the importance of analyzing NMR titration data from the perspective of microscopic pK_{Ai} values. Fortuitously, the enzyme contains only two glutamic acids, both of which serve catalytic roles in the hydrolysis of xylan via a double-displacement mechanism. Also, the core active site of the enzyme is devoid of any additional ionizable groups, except for tyrosine and arginine residues (both with expected pK_A values > 10). Summarizing the results of several previous studies (McIntosh et al. 1996; Joshi et al. 2001), at the pH optimum of $\sim$5.6 for BcX, Glu78 (with a kinetically-determined pK_A $\sim$ 4.6) is negatively-charged to function as a nucleophile, while Glu172 ("kinetic" pK_A $\sim$ 6.7) is protonated to act as a general acid. This results in a classical bell-shaped profile of activity versus pH. Upon covalent modification of Glu78 to form a trapped glycosyl-enzyme intermediate, the pK_A of Glu172 drops to $\sim$4.2, allowing it to assist a nucleophilic water molecule by general base catalysis. As explained below, studies with mutant forms of the enzyme revealed that the elevated pK_A of Glu172 is due largely to electrostatic repulsion from Glu78 (C^{δ}–C^{δ} separation = 6.5 Å). Thus,

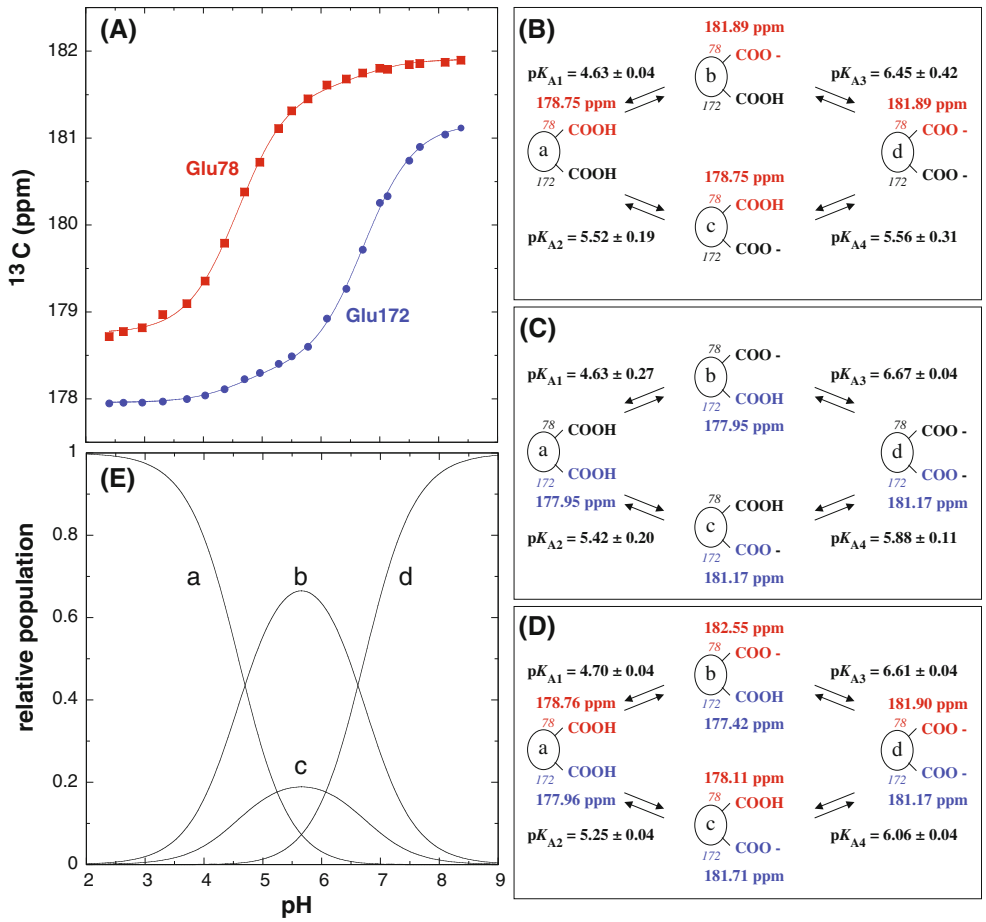

Fig. 3 Glu78 and Glu172 in BcX undergo thermodynamically coupled titrations. **a** The pH-dependent $^{13}C^{\delta}$ chemical shifts of these two residues at 25°C and ~60 mM ionic strength (25 mM sodium phosphate, 3 mM NaN_3, 10% D_2O) measured by 1D ^{13}C-NMR (taken from (McIntosh et al. 1996)). Independent fitting of these data for either **b** Glu78 or **c** Glu172 according to case 2 (5) yields the indicated microscopic pK_{Ai} values and limiting chemical shifts. The resulting interaction terms, $-\log(\alpha) = 0.94 \pm 0.32$ and 1.24 ± 0.18, corresponds to unfavorable interaction free energies of 1.28 ± 0.40 kcal/mol and 1.70 ± 0.25 kcal/mol, respectively. The pK_{Ai} values obtained from fitting each data set independently differ somewhat due to the assumption that the $^{13}C^{\delta}$ chemical shift of a residue reports only its own ionization state. **d** Also shown are the results of simultaneously fitting the titration data of both Glu78 and Glu172 to common pK_{Ai} values. In addition, the indicated chemical shift changes of the intermediate versus endpoint states were derived from measurements with the mutants E78Q and E172Q (McIntosh et al. 1996). This fitting procedure gives a slightly larger and more precisely determined common interaction free energy of 1.88 ± 0.08 kcal/mol (or $-\log(\alpha) = 1.38 \pm 0.06$). **e** The relative populations of the four possible protonation states of the carboxylic acid pair, calculated from the fit pK_{Ai} values of **e**. State *b*, with a maximum relative population of 0.67 at pH 5.66, is catalytically competent with the nucleophile Glu78 charged and the general acid Glu172 protonated

"cycling" of the pK_A of Glu172, as required for its function as a general acid and then base, results intrinsically as Glu78 cycles from carboxylate to ester along the reaction pathway.

The first clues to the occurrence of this critical electrostatic coupling were provided by the biphasic titration curves observed using one-dimensional ^{13}C-NMR measurements to study wild type BcX selectively labelled with $^{13}C^{\delta}$-glutamic acid (reproduced in Fig. 3a) (McIntosh et al. 1996). With increasing pH, the signals arising from Glu78 and Glu172 both shift downfield by ~3.1 ppm. Such behaviour is expected for the ionization of a carboxylic acid, and thus the major determinants of these pH-dependent chemical shift changes are undoubtedly the protonation/deprotonation equilibria of the glutamic acid residues themselves. Fitting these data to (11) yields macroscopic values of $pK_{AI} = \underline{4.57 \pm 0.07}$ and $pK_{AII} = 6.51 \pm 0.42$ for Glu78 and $pK_{AI} = 4.56 \pm 0.26$ and $pK_{AII} = \underline{6.74 \pm 0.05}$ for Glu172. The major titration values (underlined) agree very well with the "kinetic" p*K*a values of 4.6 and 6.7 describing the acidic and basic limbs of the pH-activity profile of the enzyme, in accordance with the assigned catalytic roles of Glu78 and Glu172. Furthermore, the complementarity of the pK_A values fit for the two residues suggested strongly that the biphasic titration curves result from their thermodynamic and/or spectroscopic interaction. This prompted the need to consider more specific microscopic models.

Microscopic pK_{Ai} values for the coupled titrations of Glu78 and Glu172 can be extracted following the assumption of case 2, in which the chemical shift of a carboxyl changes only as a consequence of the ionization of the residue itself (Fig. 3b, c). According to this analysis, Glu78 and Glu172 have microscopic pK_{Ai} values of ~4.6 and ~5.5, respectively, in the presence of neutral partner, and ~5.7 and ~6.6, respectively, in that of a charged partner. This corresponds to an unfavorable interaction free energy $\Delta G^{o}_{int} = -RT\ln(\alpha) = 2.303\ RT(\Delta pK_{Ai})$ of 1.3–1.70 kcal/mol. Importantly, $|pK_{A1} - pK_{A2}| \sim 0.9$, thus falling within the range required for branched, rather than sequential, deprotonation events.

Closer inspection of the data in Fig. 3 reveals that the titration curve of Glu172 shows more pronounced biphasic character than that of Glu78 (e.g. their normalized curves are not "mirror images"). This results in the variation of pK_{Ai} and α values determined by individually fitting the titration curves of the two residues (Fig. 3b vs. Fig. 3c). Ideally, these values should be identical. Therefore, the assumptions for case 2 must be overly restrictive, and the chemical shift of each carboxyl may also be dependent upon the charge state of its catalytic partner. To fit the titration data to the most general form of (3) additional, independent chemical shift information is required.

Fitting restraints provided by mutation of Glu78 and Glu172 in Bcx

One approach for an improved titration analysis of BcX is to consider the pH-dependent chemical shifts of the complementary mutants E78Q and E172Q in order to estimate the chemical shifts of Glu78 and Glu172 in states b and c. In the E78Q (or E172Q) mutants, the signal from the amide $^{13}C^{\delta}$ of Gln78 (or Gln172) shifts upfield by ~−0.5 ppm upon deprotonation of Glu172 (or Glu78) (McIntosh et al. 1996). Also, in these mutants, the $^{13}C^{\delta}$ carboxyl signals of Glu78 and Glu172 both shift downfield by ~3.8 ppm upon their deprotonation (or ~0.7 ppm more than in the wild type enzyme). This suggests that, for both Glu78 and Glu172, deprotonation of the partner carboxyl leads to a small change in chemical shift *opposite* in sign to that occurring for the ionization of the residue itself, thus somewhat masking the biphasic character of the observed titration curves. A similar approach of using variants to dissect chemical shift changes was exploited to analyze the microscopic pK_{Ai} values of reduced *E. coli* thioredoxin (Chivers et al. 1997).

Figure 3d shows the results of simultaneously fitting the titration curves of Glu78 and Glu172 to common microscopic pK_{Ai} values, while constraining their individual chemical shift differences between the intermediate (b and c) versus endpoint (a and d) states to averaged values measured with the E78Q and E172Q mutants. This assumes additive effects along either ionization branch. As expected, pK_{A1} and pK_{A3} for the predominant pathway remain similar to the values fit independently according to case 2 (Fig. 3b, c) or to the macroscopic model. However, inclusion of the opposing direct and indirect chemical shift effects lowers pK_{A2} for Glu172 in the presence of a neutral Glu78 to ~5.25, and raises pK_{A4} for Glu78 in the presence of charged Glu172 to ~6.06. This reveals that the electrostatic coupling between the two residues is closer to 1.88 ± 0.08 kcal/mol. It is also noteworthy that the relative populations of the singly protonated states b and c are given by the ratio K_{A1}/K_{A2} (2). Thus, based on this analysis, at the pH optimum of 5.66, BcX is 67% in the catalytically competent state with Glu78 deprotonated and Glu172 protonated, 19% in an isomeric state with the reverse charge distribution, and 7% each in the doubly protonated or deprotonated states (Fig. 3e).

In addition to providing chemical shift information, the variants of BCX with glutamine substitutions can be used to obtain independent estimates of the microscopic pK_{Ai} values of each glutamic acid in the presence of a neutral partner. As reported previously (McIntosh et al. 1996), Glu78 shows a monophasic titration in the E172Q variant and a pK_{Ai} value of 5.05 ± 0.03. In the complementary E78Q mutant, Glu172 exhibits a pK_{Ai} of 4.17 ± 0.04 (although deviating from monophasic behavior at low pH values). A similar $pK_{Ai} = 4.16 \pm 0.05$ for Glu172 was measured for the WT enzyme with Glu78 glycosylated by a mechanism-based inhibitor. The absence of second transitions in the pH range of interest supports strongly the argument that the biphasic titration curves of the two glutamic acids indeed also reflect the protonation equilibria of their catalytic partners.

In detail however, the pK_{Ai} values measured in the mutant enzymes do differ from the corresponding microscopic pK_{Ai} values fit for the WT species (Fig. 3). Based on either the above macroscopic or microscopic analyses, Glu78 has a reliable pK_{A1} of ~4.6 in the presence of a neutral Glu172, whereas the corresponding value in the E172Q species is elevated moderately to 5.05. More surprisingly, fitting of the titration data for Glu172 yields an estimated pK_{A2} of ~5.2–5.5 in the presence of a neutral Glu78, yet the measured value in the E78Q mutant drops significantly to 4.17. To some extent, these discrepancies arise from challenges in accurately fitting titration data to obtain pK_{Ai} values for minor ionization pathways. Furthermore, as shown by theoretical pK_A calculation (below), Glu78 and Glu172 are not an isolated charge system, but rather are titrating against a background of numerous other ionizable groups in BcX. However, not withstanding that the pK_{A2} for Glu172 is difficult to measure accurately, it cannot be as low as 4.17 in WT BcX simply because Glu78,

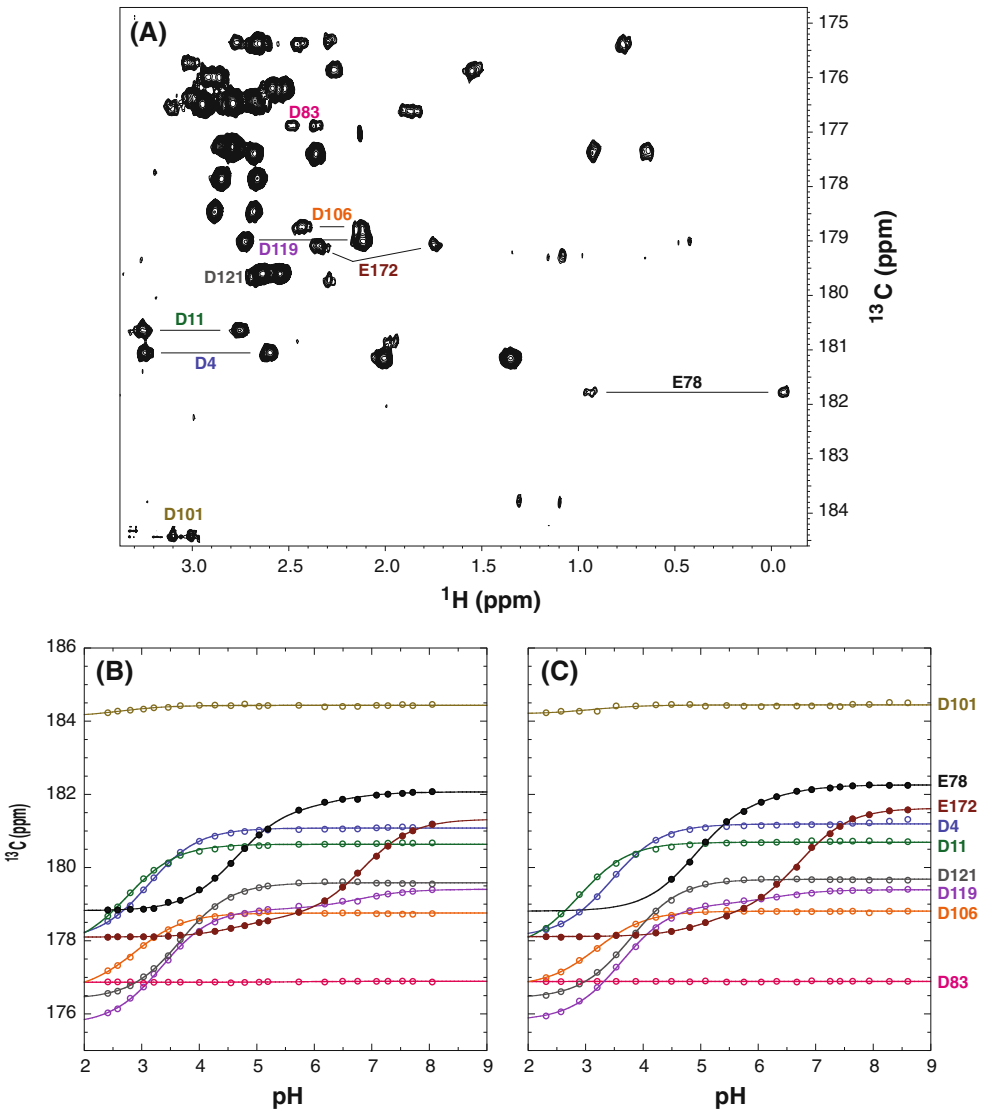

Fig. 4 **a** H_2(C)CO spectrum of ~0.7 mM $^{13}C/^{15}N$-labeled BcX (10 mM sodium phosphate, 10 mM sodium acetate, 5% D_2O buffer, pH 6.18) recorded in 75 min at 25°C with a cryoprobe-equipped Varian Inova 600 MHz NMR spectrometer. For clarity, peaks from the Asp and Glu, but not Asn and Gln, sidechains are labeled. These assignments were obtained using H(CCO)TOCSY-NH and C(CO)TOCSY-NH experiments (Sattler et al. 1999), combined with the previously reported assignments of the signals from the main chain nuclei in BcX (Plesniak et al. 1996). The pH-dependent chemical shifts of the Asp and Glu residues of BcX in the above buffer without additional salt (initially ~40 mM ionic strength) and with 500 mM NaCl (initially ~540 mM ionic strength) are shown in **b** and **c**, respectively. The *lines* are best fits to equations with 1 or 2 macroscopic pK_A values (Table 1)

with a well established pK_{A1} of ~4.6, clearly deprotonates first with increasing pH. This indicates that the mutations may also lead to structural, as well as electrostatic changes, in BcX and are not exact mimics of a neutral glutamic acid, either in terms of providing pK_{Ai} or chemical shift information. Thus, to the first approximation, the study of mutant species can provide excellent qualitative support for arguments, such as that of electrostatic coupling, based on the fitting of NMR-derived titration data for a wild type protein. However, caution must be exercised as quantitative differences may arise due to additional perturbations introduced by the amino acid substitution.

Ionic strength-dependent electrostatic interactions in BcX

The postulated thermodynamic coupling between the ionization equilibria of Glu78 and Glu172 is expected to vary with the sample ionic strength. Therefore, we measured the pH-dependent chemical shifts of the Glu and Asp residues in BcX with low (~40 mM) and high (~540 mM) ionic strength buffers. Unlike our original studies using one-dimensional ^{13}C-NMR of selectively $^{13}C^{\delta}$-Glu (McIntosh et al. 1996) or $^{13}C^{\gamma}$-Asp (Joshi et al. 1997) labeled BcX, these measurements were carried out using a two-dimensional H_2(C)CO experiment with uniformly ^{13}C-labeled protein (Fig. 4). The fit macroscopic pK_A values are summarized in Table 1. The values obtained from the current low ionic strength sample (~40 mM) agree well with those reported previously (~60 mM ionic strength; Joshi et al. 1997), yet tend to be systematically higher by ~0.1–0.2 units. In contrast to the generally small errors in the *precision* of data fitting, this variation between samples and experimental protocols provides a more reasonable estimate of the *accuracy* by which pK_A values can actually be measured.

Table 1 Ionic strength-dependent macroscopic pK_A values of BcX

Residue	Low ionic strength[a]	High ionic strength[b]
Glu78[c]	4.61 ± 0.07 and 6.40 ± 0.41	4.86 ± 0.20 and 6.54 ± 0.48
Glu172[c]	4.68 ± 0.21 and 6.85 ± 0.06	5.07 ± 0.24 and 6.74 ± 0.07
Asp4[d]	3.10 ± 0.05	3.41 ± 0.05
Asp11[d]	2.65 ± 0.13	2.75 ± 0.16
Asp83[e]	<2	<2
Asp101[e]	<2	<2
Asp106[d]	2.90 ± 0.12	3.21 ± 0.10
Asp119[f]	3.35 ± 0.04	3.62 ± 0.05
Asp121[g]	3.67 ± 0.03	3.78 ± 0.09

[a] Samples in 10 mM sodium phosphate, 10 mM sodium d_3-acetate, 5% D_2O buffer (initial ionic strength ~ 40 mM) at 25°C

[b] Samples in the above buffer with 500 mM NaCl (initial ionic strength ~ 540 mM)

[c] Underlined is the pK_{AI} or pK_{AII} value associated with the predominant change in chemical shift when fit to the equation for two macroscopic ionizations. See Fig. 5 for fitting according to a microscopic model

[d] Predominant pK_{AI} value ($\Delta\delta$ ~ 3 ppm) when fit to the equation for two macroscopic ionizations. A second pK_{AII} value (> 5) corresponds to a small chemical shift change (< 0.2 ppm) and is not listed

[e] No observed titration between pH ~ 2.3 and 8.6. The lack of a deuterium isotope shift confirms both Asp83 and Asp101 are deprotonated in the native protein (Joshi et al. 1997)

[f] Asp119 shows a visibly biphasic titration. The tabulated pK_{AI} ($\Delta\delta$ ~ 3.2 ppm) is attributed to the deprotonation of Asp119 itself. The second pK_{AII} value of 6.77 ± 0.16 (low ionic strength) and 6.34 ± 0.19 (high) correspond to smaller chemical shift changes of ~0.5 ppm. Asp119 is in the "thumb" region of Bcx, over its active site, and thus the latter may result from a conformational change due to deprotonation of Glu172 ($C^{\delta} - C^{\gamma}$ ~ 17 Å between Asp119 and Glu172)

[g] Fit to a single acid dissociation equilibrium

The titration curves of Glu78 and Glu172 recorded at high ionic strength are still biphasic, yet not as visibly pronounced as at low ionic strength (Fig. 5). Simultaneous fitting of these data to the model of case 2 yields the microscopic pK_{Ai} values also summarized in this figure. Comparison with Fig. 3 reveals that both the pK_{A1} and pK_{A2} values (ionization of Glu78 and Glu172 in the presence of a neutral neighbor) increased at higher salt concentrations. This could reflect a screening of stabilizing electrostatic interactions with the positively-charged lysine, arginine, and histidine residues of BcX. In support of this argument, the pK_A values of all the aspartic acid residues in BcX also increased with increasing sample ionic strength (Table 1), thereby closer approaching model compound pK_A values of ~3.9 (Pace et al. 2009). However, pK_{A3}, which corresponds to the deprotonation of Glu172 in the presence of a charged Glu78, did not change upon additional of salt. This appears to be the net effect of an increased pK_{A2} value offset by reduced unfavorable interactions with Glu78. Indeed, the fit interaction free energy decreased from ~1.7 to ~1.2 kcal/mol with increased sample ionic strength. Overall, this supports the argument that the biphasic titrations of Glu78 and Glu172 result in large part from their thermodynamic coupling.

Theoretical electrostatic calculations for BcX

Complementing experimental measurements on wild type and mutant forms of BcX, we also carried out theoretical pK_A calculations as an avenue for understanding the electrostatic interactions within this enzyme. Figure 6 present the theoretical "titration curves" (charge vs. pH) for Glu78 and Glu172 in wild type BcX. Based on a practical definition of 50% ionization, the apparent $pK_{A1/2}$ values for these two residues were calculated to be ~2.9 and 5.9, respectively. Although systematically lower than the experimental values of 4.6 and 6.7, respectively, these numbers do recapitulate the key point that Glu78 ionizes more readily than Glu172, in accordance with their catalytic roles. (The discrepancies between the experimental and calculated pK_A values and interaction energies are a result of using a fixed protein dielectric constant of 8. This produces the best overall agreement with a large set of experimental pK_A values measured for many proteins, yet may not be appropriate for BcX.) Most importantly, the calculated titration curves deviate substantially from monophasic behaviour due primarily to a theoretical electrostatic coupling of 2.3 kcal/mol between these two residues. The effect of this coupling is verified by the absence of the pronounced "shoulder" in the titration curve of each glutamic acid calculated when its partner has a charge fixed at either −1 or 0 (not shown).

Since these theoretical data are not complicated by issues of chemical shift interpretation, microscopic pK_{Ai} values can be extracted by fitting to (15) describing the fractional negative charge (f_-) of a carboxyl coupled to one other ionizable residue:

$$f_- = \frac{\left(10^{-(\mathrm{pH}+\mathrm{p}K_{A1})} + 10^{-(\mathrm{p}K_{A1}+\mathrm{p}K_{A3})}\right)}{10^{-2(\mathrm{pH})} + 10^{-(\mathrm{pH}+\mathrm{p}K_{A2})} + 10^{-(\mathrm{pH}+\mathrm{p}K_{A1})} + 10^{-(\mathrm{p}K_{A1}+\mathrm{p}K_{A3})}} \quad (15)$$

Results of these fittings are presented in Fig. 6. This analysis reveals that with increasing pH, Glu78 predominantly deprotonates first with $pK_{A1} = 2.77$ followed by Glu172 with $pK_{A3} = 5.99$. However, an alternative pathway involves Glu172 ionizing initially with $pK_{A2} = 3.63$, followed by Glu78 with $pK_{A3} = 5.13$. The similarity to the analysis of Fig. 3 supports our interpretation of the NMR-derived titration curves of BcX in terms of a branched ionization pathway.

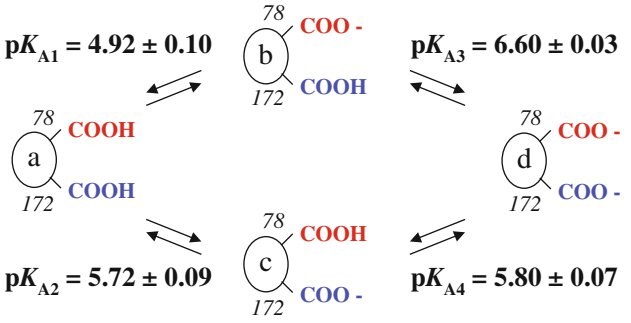

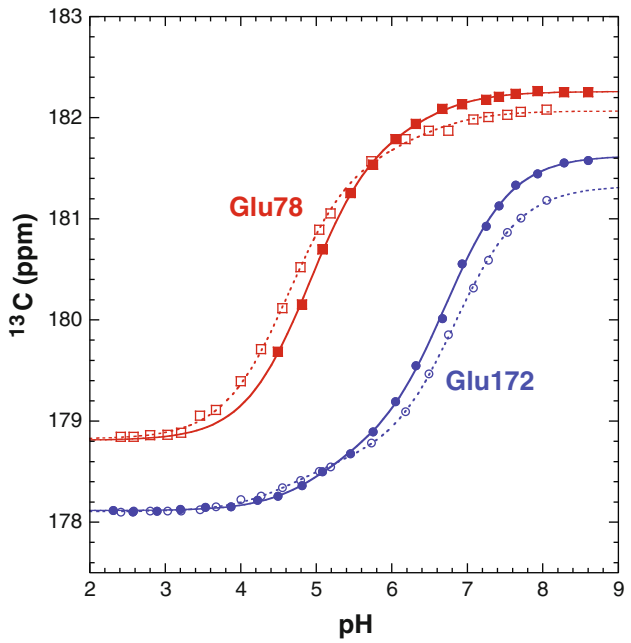

Fig. 5 Increased ionic strength decreases the electrostatic coupling between Glu78 and Glu172, as reflected by a reduction in the biphasic character of their titration curves. *Lower* $^{13}C^{\delta}$ chemical shift versus pH for Glu78 and Glu172 at low (~40 mM; *open symbols* and *dashed fit lines*) and high (~540 mM; *closed symbols* and *solid fit lines*) ionic strength. These data were re-plotted from Fig. 4. Unfortunately, Glu78 yields a weak $H_2(C)CO$ signal that is not detected at low pH values and elevated salt conditions. *Upper* The results of simultaneously fitting the titration data of both Glu78 and Glu172 at high ionic strength to common microscopic pK_{Ai} values. Independent chemical shifts were assumed as mutant data were unavailable under these conditions. Fitting at the titration data recorded at low ionic strength yields values similar to those in Fig. 3 ($pK_{A1} = 4.69 \pm 0.03$, $pK_{A2} = 5.48 \pm 0.05$, $pK_{A3} = 6.73 \pm 0.04$, and $pK_{A4} = 5.94 \pm 0.06$; not shown). The resulting interaction terms, $-\log(\alpha) = 1.25 \pm 0.07$ and 0.88 ± 0.09, correspond to unfavorable interaction free energies of 1.71 ± 0.10 kcal/mol and 1.20 ± 0.13 kcal/mol, at low and high ionic strength, respectively

Fig. 6 Theoretical calculations confirm that Glu78 and Glu172 in BcX undergo electrostatically coupled titrations. *Lower* Predicted average charges of Glu78 (*open square*) and Glu172 (*open circle*) versus pH value. Fitting to single titrations yields unsatisfactory pK_A values of 2.92 ± 0.03 for Glu78 and 5.87 ± 0.03 for Glu172 (4; not shown). In contrast, the lines result from simultaneous fitting to a model of two coupled ionizable groups using (15). The mean and standard deviations of the fit common microscopic pK_{Ai} values are indicated in the upper schematic. The interaction term $-\log(\alpha) = 2.36 \pm 0.06$ derived from these pK_{Ai} values corresponds to an unfavorable interaction free energy of 3.2 ± 0.08 kcal/mol. This is larger than the theoretical value of 2.3 kcal/mol due to the influence of additional titratable residues in BcX, which lead to the visible discrepancies between the data points and fit curves. The inflection points on the fit titration curves occur at pH values equal to the macroscopic $pK_{AI} = -\log(K_{A1} + K_{A2}) = 2.71$ and $pK_{AII} = -\log((K_{A3}^{-1} + K_{A4}^{-1})^{-1}) = 6.04$. The mid-point plateaus at charges of $-K_{A1}/(K_{A1} + K_{A2}) = -0.88$ and $-K_{A2}/(K_{A1} + K_{A2}) = -0.12$ for Glu78 and Glu172, respectively, reflect the relative tendency for deprotonation along the upper versus lower pathway

Closer inspection of the data in Fig. 3 reveals that the titration curves calculated for Glu78 and Glu172 are not mirror images of one another and that they cannot be completely fit to a simple model of two ionizable groups. Furthermore, the coupling 3.21 ± 0.08 kcal/mol derived from the fit microscopic pK_{Ai} values is significantly larger than the theoretical interaction term of only 2.3 kcal/mol. These differences arise as Glu78 and Glu172 are not an isolated system, but rather lie within a protein containing seven aspartic acids, two histidines, and a C-terminus that also titrate under acidic pH conditions (Joshi et al. 1997).

Collectively, these small pH-dependent electrostatic interactions contribute to the "shoulders" on the titrations curves of Fig. 6. This in turn will bias fitting of the pK_{Ai} values associated with the minor ionization pathway of the simplified two carboxylic acid model and lead to difficulties in accurately determining the interaction term α. This illustrates a fundamental difficulty in attempting to quantitate electrostatic interactions between specific residues within a protein by either theoretical or experimental methods. Since an acid dissociation constant can only be measured under conditions when both the protonated and deprotonated forms of a residue are populated at detectable levels (e.g. $|pH - pK_{Ai}| < 2$), pK_{Ai} values of different residues are generally determined in the context of different electrostatic backgrounds. Hence the model of Fig. 1 is inherently an approximation for any protein. Indeed, Lindman et al. analyzed the NMR-monitored titration curves of the B1 domain of protein G in terms of "pH-dependent pK_A values" (Lindman et al. 2006).

Summary

In this study, we have revisited the example of two interacting carboxylic acid residues in order to establish guidelines for analyzing the NMR-monitored pH titration curves of the catalytic residues in BcX. Despite the apparent simplicity of this minimalistic model, the possibility that the two residues are coupled both thermodynamically and spectroscopically leads to experimentally underdetermined titration curves. In the absence of any additional information, the contributions of these two effects cannot be separated. Therefore, in the strictest sense, fitting biphasic titration curves will only yield *macroscopic* pK_A values and intermediate chemical shifts that reflect the combined ionization equilibria of *both* residues in this model xylanase. However, under favorable circumstances, summarized below, it is also possible to analyze these titration curves to obtain *microscopic* pK_{Ai} values and thus a measure of the electrostatic interaction energy between the two catalytic residues in this enzyme.

Fitting of the titration curves for Glu78 and Glu172 to yield the microscopic pK_{Ai} values summarized in Figs. 3 and 5 is justified for the following reasons. First, the two residues are closely juxtaposed within the active site of the enzyme and thus are expected to interact with one another. That is, the analysis is physicochemically reasonable. Second, the fit pK_{A1} and pK_{A2} values are comparable, as required for both singly protonated species to occur with measureable populations. Third, each residue shows a monophasic titration when the other is mutated to a glutamine or, in the case of Glu78, covalently modified with a mechanism-based inhibitor (McIntosh et al. 1996). These mutants also provide chemical shift information that enables a more accurate fitting of the titration curves to a microscopic model. Fourth, the titration curves of Glu78 and Glu172 appear more Henderson-Hasselbalch-like with increased ionic strength and therefore reduced electrostatic coupling. And fifth, theoretical calculations also recapitulate the coupled ionization equilibria of the two residues.

Collectively, these results help explain the pH-dependent mechanism of BcX and the catalytic roles of its two active site residues. In summary, the kinetically-determined pK_A values of $\sim$4.6 and $\sim$6.7 governing the bell-shaped activity profile (k_{cat}/K_m versus pH) of this model xylanase match closely the macroscopic pK_A values of 4.57 and 6.74 extracted for Glu78 and Glu172 from NMR-monitored pH titrations. This is consistent with their roles as a nucleophile and general acid, respectively, in the glycosylation step of the double-displacement mechanism of BcX. A more detailed analysis of the biphasic titration curves of the two residues according to a model of two coupled ionizations also reveals microscopic pK_{Ai} values of 4.70 (and 6.06) for Glu78 and 5.25 (and 6.61) for Glu172 in the presence of their neutral (and charged) catalytic partner. Thus, the elevated pK_{A3} value of Glu172 in the catalytically-competent protonation state of BcX results in part from an unfavorable electrostatic coupling of $\sim$1.9 kcal/mol with the negatively-charged nucleophile Glu78. Upon formation of the glycosyl-enzyme intermediate, Glu78 is covalently modified and their electrostatic coupling is eliminated. This allows the pK_A value of Glu172 to drop, thereby enabling this residue to serve as a general base, activating a nucleophilic water and facilitating the subsequent deglycosylation step of the hydrolytic reaction. The intrinsic "pK_A cycling" of the general acid/base Glu172 in response to electrostatic changes along the reaction pathway of BcX illustrates beautifully the elegance by which enzymes have evolved to catalyze biochemical reactions.

Acknowledgments We are grateful Lewis Kay for friendship, expert advice, and countless pulse sequences, without which none of our work would be possible. Yom Huledet Same'ach! We also thank Rick Dahlquist and Steve Withers for insightful comments and Philip Johnson for early experimental help. This research was funded by the Natural Sciences and Engineering Research Council of Canada (NSERC; to LPM). Instrument support was provided by the Canadian Institutes for Health Research (CIHR), the Canadian Foundation for Innovation (CFI), the British Columbia Knowledge Development Fund (BCKDF), the UBC Blusson Fund, and the Michael Smith Foundation for Health Research (MSFHR).

References

Alberty RA (2000) Effect of pH on protein-ligand equilibria. J Phys Chem B 104:9929–9934

Andre I, Linse S, Mulder FAA (2007) Residue-specific pK(a) determination of lysine and arginine side chains by indirect ^{15}N and

^{13}C NMR spectroscopy: application to apo calmodulin. J Am Chem Soc 129:15805–15813

Batchelor JG, Feeney J, Roberts GCK (1975) C-13 NMR protonation shifts of amines, carboxylic-acids and amino-acids. J Mag Reson 20:19–38

Blomberg F, Maurer W, Ruterjans H (1977) Nuclear magnetic-resonance investigation of ^{15}N -labeled histidine in aqueous-solution. J Am Chem Soc 99:8149–8159

Buckingham AD (1960) Chemical shifts in the nuclear magnetic resonance spectra of molecules containing polar groups. Can J Chem 38:300–307

Chivers PT, Prehoda KE, Volkman BF, Kim BM, Markley JL, Raines RT (1997) Microscopic pK(a) values of *Escherichia coli* thioredoxin. Biochemistry 36:14985–14991

Creighton TE (2010) The biophysical chemistry of nucleic acids and proteins. Helvetian Press

Delaglio F, Grzesiek S, Vuister GW, Zhu G, Pfeifer J, Bax A (1995) NMRpipe—a multidimensional spectral processing system based on Unix pipes. J Biomol NMR 6:277–293

Edsall JT, Wyman J (1958) Biophysical chemistry. Academic Press, New York

Farrell D, Miranda ES, Webb H, Georgi N, Crowley PB, McIntosh LP, Nielsen JE (2010) Titration_DB: storage and analysis of NMR-monitored protein pH titration curves. Proteins Struct Func Bioinf 78:843–857

Goddard TD, Kneller DG (2004) Sparky 3. University of California, San Francisco

Hass MA, Jensen MR, Led JJ (2008) Probing electric fields in proteins in solution by NMR spectroscopy. Proteins 72:333–343

Hooft RWW, Sander C, Vriend G (1996) Positioning hydrogen atoms by optimizing hydrogen-bond networks in protein structures. Proteins Struct Func Gen 26:363–376

Joshi MD, Hedberg A, McIntosh LP (1997) Complete measurement of the pK(a) values of the carboxyl and imidazole groups in *Bacillus circulans* xylanase. Prot Sci 6:2667–2670

Joshi MD, Sidhu G, Nielsen JE, Brayer GD, Withers SG, McIntosh LP (2001) Dissecting the electrostatic interactions and pH-dependent activity of a family 11 glycosidase. Biochemistry 40:10115–10139

Kay L (1993) Pulsed-field gradient-enhanced three-dimensional NMR experiment for correlating $^{13}C\alpha/\beta$, $^{13}C'$, and $^{1}H\alpha$ chemical shifts in uniformly ^{13}C labelled proteins dissolved in H_2O. J Am Chem Soc 115:2055–2057

Klingen AR, Bombarda E, Ullmann GM (2006) Theoretical investigation of the behavior of titratable groups in proteins. Photochem Photobiol Sci 5:588–596

Lindman S, Linse S, Mulder FAA, Andre I (2006) Electrostatic contributions to residue-specific protonation equilibria and proton binding capacitance for a small protein. Biochemistry 45:13993–14002

Markley JL (1975) Observation of histidine residues in proteins by means of nuclear magnetic-resonance spectroscopy. Acc Chem Res 8:70–80

McIntosh LP, Hand G, Johnson PE, Joshi MD, Korner M, Plesniak LA, Ziser L, Wakarchuk WW, Withers SG (1996) The pK(a) of the general acid/base carboxyl group of a glycosidase cycles during catalysis: a ^{13}C-NMR study of *Bacillus circuluns* xylanase. Biochemistry 35:9958–9966

Nielsen JE (2009) Analyzing enzymatic pH activity profiles and protein titration curves using structure-based pKa calculations and titration curve fitting. Methods Enzymol 454:233–258

Nielsen JE, Andersen KV, Honig B, Hooft RWW, Klebe G, Vriend G, Wade RC (1999) Improving macromolecular electrostatics calculations. Prot Eng 12:657–662

Oda Y, Yamazaki T, Nagayama K, Kanaya S, Kuroda Y, Nakamura H (1994) Individual ionization-constants of all the carboxyl groups in ribonuclease Hi from *Escherichia-coli* determined by NMR. Biochemistry 33:5275–5284

Onufriev A, Case DA, Ullmann GM (2001) A novel view of pH titration in biomolecules. Biochemistry 40:3413–3419

Pace CN, Grimsley GR, Scholtz JM (2009) Protein ionizable groups: pK values and their contribution to protein stability and solubility. J Biol Chem 284:13285–13289

Pelton JG, Torchia DA, Meadow ND, Roseman S (1993) Tautomeric states of the active-site histidines of phosphorylated and unphosphorylated Iii(Glc), a signal-transducing protein from *Escherichia coli*, using 2-dimensional heteronuclear NMR techniques. Prot Sci 2:543–558

Plesniak LA, Wakarchuk WW, McIntosh LP (1996) Secondary structure and NMR assignments of *Bacillus circulans* xylanase. Prot Sci 5:1118–1135

Quirt AR, Lyerla JR, Peat IR, Cohen JS, Reynolds WF, Freedman MH (1974) ^{13}C Nuclear magnetic-resonance titration shifts in amino-acids. J Am Chem Soc 96:570–571

Rabenstein DL, Sayer TL (1976a) ^{13}C Chemical-shift parameters for amines, carboxylic-acids, and amino-acids. J Mag Reson 24: 27–39

Rabenstein DL, Sayer TL (1976b) Determination of microscopic acid dissociation-constants by nuclear magnetic-resonance spectrometry. Anal Chem 48:1141–1145

Rouxfromy M (1982) On the hill plot of NMR data for titration of protein residues. Biophys Struct Mech 8:289–306

Sattler M, Schleucher J, Griesinger C (1999) Heteronuclear multidimensional NMR experiments for the structure determination of proteins in solution employing pulsed field gradients. Prog Nucl Mag Reson Spec 34:93–158

Shrager RI, Sachs DH, Schechte A, Cohen JS, Heller SR (1972) Nuclear magnetic-resonance titration curves of histidine ring protons. 2. Mathematical models for interacting groups in nuclear magnetic-resonance titration curves. Biochemistry 11:541–547

Sondergaard CR, McIntosh LP, Pollastri G, Nielsen JE (2008) Determination of electrostatic interaction energies and protonation state populations in enzyme active sites. J Mol Biol 376: 269–287

Sudmeier JL, Reilley CN (1964) Nuclear magnetic resonance studies of protonation of polyamine + aminocarboxylate compounds in aqueous solution. Anal Chem 36:1698

Surprenant HL, Sarneski JE, Key RR, Byrd JT, Reilley CN (1980) ^{13}C NMR-studies of amino-acids—chemical-shifts, protonation shifts, microscopic protonation behavior. J Mag Reson 40: 231–243

Szakacs Z, Kraszni M, Noszal B (2004) Determination of microscopic acid-base parameters from NMR-pH titrations. Anal Bioanal Chem 378:1428–1448

Tomlinson JH, Green VL, Baker PJ, Williamson MP (2010) Structural origins of pH-dependent chemical shifts in the B1 domain of protein G. Proteins Struct Func Bioinf 78:3000–3016

Ullmann GM (2003) Relations between protonation constants and titration curves in polyprotic acids: a critical view. J Phys Chem B 107:1263–1271

Wang ZX (1995) An exact mathematical expression for describing competitive-binding of 2 different ligands to a protein molecule. FEBS Lett 360:111–114

Webb H, Tynan-Connolly BM, Lee GM, Farrell D, O'Meara F, Sondergaard CR, Teilum K, Hewage C, McIntosh LP, Nielsen JE (2011) Remeasuring HEWL pK(a) values by NMR spectroscopy: methods, analysis, accuracy, and implications for theoretical pK(a), calculations. Proteins Struct Func Bioinf 79:685–702

Yang AS, Gunner MR, Sampogna R, Sharp K, Honig B (1993) On the calculation of pK(a)s in proteins. Proteins Struc Func Gene 15:252–265